Superconductor Science and Technology

PAPER • OPEN ACCESS

Electromagnetic strain measurements and two-directional mechanical stress estimation for a REBaCuO ring bulk reinforced by a metal ring during field-cooled magnetization

To cite this article: Sora Namba *et al* 2019 *Supercond. Sci. Technol.* **32** 125011

OPEN ACCESS
IOP Publishing
Superconductor Science and Technology
Supercond. Sci. Technol. **32** (2019) 125011 (10pp)
https://doi.org/10.1088/1361-6668/ab4a8b

Electromagnetic strain measurements and two-directional mechanical stress estimation for a REBaCuO ring bulk reinforced by a metal ring during field-cooled magnetization

Sora Namba[1,3], Hiroyuki Fujishiro[1], Tomoyuki Naito[1], Mark D Ainslie[2] and Kai Y Huang[2]

[1] Department of Physical Science and Materials Engineering, Faculty of Science and Engineering, Iwate University, 4-3-5 Ueda, Morioka 020-8551, Japan
[2] Department of Engineering, University of Cambridge, Trumpington Street, Cambridge CB2 1PZ, United Kingdom

E-mail: g0318128@iwate-u.ac.jp

Received 1 April 2019, revised 20 September 2019
Accepted for publication 3 October 2019
Published 4 November 2019

Abstract

In this paper, simultaneous measurements of the electromagnetic strains along both the circumferential (θ) and radial (r) directions are reported for a large single-grain EuBaCuO ring bulk reinforced by an Al alloy ring during field-cooled magnetization (FCM) from 5 T at 50 K using several strain gauges adhered to the surface. To verify the experimental results and to understand the complex stress–strain behavior, mechanical analyses were carried out using a three-dimensional finite element model that closely represents the experimental setup. The simulation results of the electromagnetic strains along both directions showed excellent qualitative and quantitative agreement with the experimental ones. These results strongly suggest that the numerical model must include the exact same structure (size, shape and materials) of the mechanical support structure as the experimental setup in order to reproduce the experimental results both qualitatively as well as quantitatively. This also explains our previous research (SuST 2019 **32** 015007), where the measured circumferential strains were about 50% smaller those in the numerical simulation. Furthermore, the electromagnetic stresses along both directions during the FCM process are estimated from the obtained experimental strains. As a result, the estimated stresses were fairly consistent with those obtained by the numerical simulations, suggesting that our stress–strain simulation technique is both qualitatively and quantitatively reliable and useful to clarify the possibility of mechanical fracture of bulk superconductors.

Keywords: bulk superconductors, trapped field magnet, mechanical stress, strain gauge measurement, numerical simulation, finite element method

(Some figures may appear in colour only in the online journal)

[3] Author to whom any correspondence should be addressed.

1. Introduction

Large, single-grain REBaCuO (RE: a rare earth element or Y) bulk superconductors are a promising material for use as a compact, high-strength trapped field magnet (TFM) [1] for various practical applications, such as rotating machines, magnetic separation, flywheel energy storage systems and so on [2–4]. REBaCuO bulks can generate magnetic fields much higher than conventional Nd–Fe–B permanent magnets or other superconducting TFMs using MgB_2 [5] and iron-pnictide [6]. In general, the trapped magnetic field capability of the bulk superconductor is proportional to both the critical current density, J_c, and bulk radius, r, based on the Bean's critical state model [7]. Until now, the increase of J_c and the enlargement of r of the bulk have been carried out over the past three decades by the improved fabrication techniques, particle refinement of the secondary phases, suppression of defect formation, and the introduction of stronger pinning centers.

Besides the enhancement of the magnetic flux pinning performance in the bulks, the mechanical reinforcement of the bulk is also an important issue during field-cooled magnetization (FCM), especially for fields of several Tesla or more. A large Lorentz force is exerted in the bulk, which sometimes results in crack formation and propagation, leading to eventual mechanical failure. This is because the REBaCuO bulk material is intrinsically a brittle ceramic with relatively low mechanical strength. In previous studies, crack formation and/or serious fracture occurred in a bulk without external reinforcement during ramped down from a high external magnetic field [8–10]. In this sense, the maximum trapped field capability is not restricted by the electromagnetic properties, but by their poor mechanical performance. Using mechanical reinforcement by shrink-fit stainless steel or epoxy resin impregnation, trapped magnetic fields over 17 T have been achieved below 30 K in disc bulk pairs [11, 12]. In addition, a ring-shaped REBaCuO bulk with a large bore has been also applied for the compact and cryogen-free NMR/MRI magnet [13, 14]. Trapped field enhancement with spatial homogeneity of ppm order is an ongoing challenge for improving resolution; a trapped field of as high as 10 T is necessary to realize a 400 MHz (9.4 T) NMR bulk magnet system. The mechanical strength of the bulk materials has usually been estimated using three-point or four-point bending tests [15–18] and tensile tests [19, 20], from which the fracture strength of a typical Ag-doped REBaCuO bulk is suggested to be as low as 50–70 MPa.

Analytical investigations of mechanical properties have been reported for disc- and ring-shaped bulks with infinite height during FCM or zero-field-cooled magnetization [8, 21–24]. On the other hand, we have reported numerical simulation results of the mechanical stress behavior for REBaCuO disc- and ring-shaped bulks with finite height and the metal ring reinforcement during FCM [25–27] using the finite element method (FEM). Furthermore, we have proposed a new reinforcement method to prevent bulk failure under higher fields [28–30].

Mechanical strain measurement using a strain gauge is a conventional and effective method for the evaluation of the local mechanical properties of a large bulk without cutting it. The electromagnetic strain, ε, in the REBaCuO disc bulk caused by the Lorentz force during FCM was directly measured on the bulk surface, and the fracture strength was estimated [31]. Recently, we have reported the electromagnetic strain along the circumferential (θ) direction of a REBaCuO ring bulk reinforced by a metal ring during FCM, and the cooling strains during the cooling process from room temperature to 50 K [32]. These experimental results were compared with numerical simulation results, in which the simple three-dimensional (3D) model consisted of the ring bulk and the reinforcement metal ring. The numerical results of the time-step dependence of the strain during FCM reproduced the experimental ones qualitatively. However, the absolute value of the experimental strain was about 50% smaller than that of the simulated one. We concluded, in the paper, that the difference mainly comes from the simulation results, which was closely related with the assumed $J_c(B)$ characteristics, and/or from the experimental strain results, which result from the existence of the macroscopic and microscopic structural inhomogeneity. The quantitative difference in the electromagnetic strain between the experiments and simulations is a serious problem, because the agreement guarantees the reliability of our numerical simulation results. We hypothesized that the difference mainly comes from an insufficient numerical model; that is, the exact same structure (size, shape and materials) of the mechanical support structure as the experimental setup must be included in the model. In addition, to enhance the reliability of the simulation results, the simultaneous measurement and verification of the electromagnetic stresses along two directions is provided.

In this paper, we measured the electromagnetic strains along both circumferential (θ) and radial (r) directions of a EuBaCuO ring bulk reinforced by an aluminum (Al) alloy ring during FCM from 5 T at 50 K using several strain gauges. The electromagnetic stresses in both directions are estimated analytically at each position from the experimental results obtained by the strain measurement using Hooke's law. A full 3D finite element model based on the actual experimental setup was developed to understand the complex stress–strain behavior of the ring bulk. The quantitative agreement between the experiments and simulations can prove the validity of our experiment and simulation techniques and validates the simulation as a reliable tool to investigate the possibility of mechanical fracture of bulk superconductors.

2. Experimental procedure

2.1. Experimental setup and FCM process

Figure 1(a) shows the experimental setup of the ring bulk with a metal ring for FCM. The EuBaCuO ring bulk (64 mm OD, 28 mm ID, and 20 mm height (H)) containing 10 wt% silver (Ag) was fabricated using a modified quench and melt growth method by Nippon Steel Corporation, Japan [33, 34]. An Al alloy reinforcement ring (A7075-T6) with the same height as the ring bulk (74 mm OD, 64.1 mm ID, and 20 mm H) was bonded to the outer peripheral surface of the ring bulk using Stycast™ 1266 epoxy resin (0.05 mm in thickness). This ring applies a compressive stress to the ring bulk during the cooling process due to the difference in the thermal contraction coefficient between two materials. The ring bulk with the Al alloy ring was tightly sandwiched by top (12 mm in thickness) and bottom (22 mm in thickness) Cu plates made of oxygen-free high-conductivity copper (OFHC Cu) using a bolt and nut. Thin indium sheets were inserted

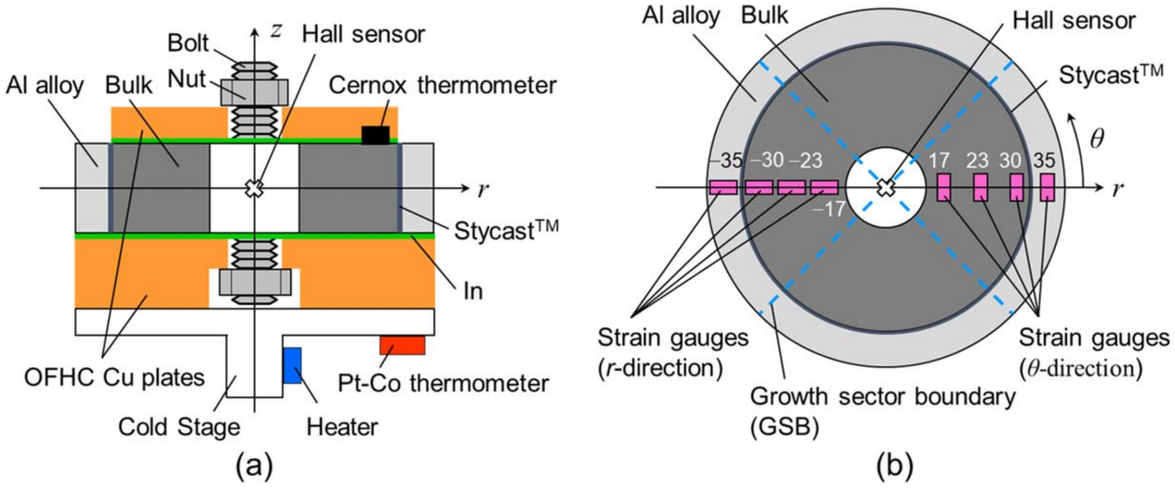

Figure 1. (a) Experimental setup of the EuBaCuO ring bulk on the cold stage of refrigerator during FCM, in which the ring bulk was sandwiched between OFHC Cu plates using a bolt and nuts. (b) Positions and directions of the strain gauges adhered to the top surface of the ring bulk and Al alloy ring.

between the bulk and both Cu plates to obtain good thermal contact. The bottom Cu plate was thermally connected to the cold stage of a Gifford-McMahon helium refrigerator. The temperature of the cold stage was controlled by a Pt–Co thermometer and a heater, attached to bottom surface of the cold stage. A straight and long groove (64 mm in length, 10 mm in width and 5 mm in depth) was made on the bottom surface of the top Cu plate to prevent mechanical contact between the Cu plate and strain gauges and to set a CERNOX™ thermometer to monitor the temperature of the bulk on the outer edge of the bulk surface. The trapped field, B_z, at the center of the ring bulk ($r = z = 0$) was measured by an axial-type Hall sensor (F. W. Bell, BHA-921). The bulk sheathed in a vacuum chamber was inserted into a cryocooled 10 T superconducting solenoid magnet (Japan Superconductor Technology, JMTD-10T100) and an external magnetic field of $B_{app} = 5$ T, parallel to z-axis, was applied to the bulk at 100 K, and then the bulk was slowly cooled to 50 K under the magnetic field of 5 T. Finally, the external magnetic field was ramped down to zero at a rate of -0.222 T min^{-1}.

2.2. Strain measurement

Figure 1(b) shows the measurement positions of the strain gauges adhered to the top surface of the EuBaCuO ring bulk and the Al alloy ring during the FCM process. Eight strain gauges (Tokyo Sokki, CFLA-1-350-11, (gauge length: 1 mm, gauge factor: $F = 2.09$)) were adhered linearly on the top surface using an epoxy adhesive (Tokyo Sokki, EA-2A). Four gauges were adhered at $r = 17$, 23, 30 mm on the bulk and at $r = 35$ mm on the Al alloy ring from the center of the bulk annuli in the growth sector region to measure the electromagnetic strain, ε_θ, along the θ-direction. The other four gauges were also adhered at symmetric positions of $r = -17$, -23, -30 and -35 mm to measure the electromagnetic strain, ε_r, along the r-direction.

The electromagnetic strain along the θ-direction, $\varepsilon_\theta = dL_\theta/L_\theta(0)$, is expressed by the following equation [32]

$$\varepsilon_\theta = \frac{dL_\theta}{L_\theta(0)} = \frac{L_\theta(B) - L_\theta(0)}{L_\theta(0)} = \frac{1}{F}\frac{dR}{R}, \tag{1}$$

where $dL_\theta = L_\theta(B) - L_\theta(0)$ is the change of length along the θ-direction by magnetic field, $L_\theta(0) = 2\pi r$ is the original length of the bulk at $B_{ex} = 0$ along the θ-direction, r is the radial measurement position on the bulk surface. The electromagnetic strain along the r-direction, $\varepsilon_r = dL_r/L_r(0)$, is expressed by the following equation

$$\varepsilon_r = \frac{dL_r}{L_r(0)} = \frac{L_r(B) - L_r(0)}{L_r(0)} = \frac{1}{F}\frac{dR}{R}, \tag{2}$$

where $dL_r = L_r(B) - L_r(0)$ is the change of length along the r-direction under the magnetic field, and $L_r(0) = r$ at $B_{ex} = 0$. The ε_θ and ε_r values on the surface were calculated by the ratio of dR/R shown in equations (1) and (2), in which R (=350 Ω) is the initial resistance of the strain gauge and $dR = R(B) - R(0)$ is the change in resistance due to the electromagnetic strain under magnetic field variation. The R (B) value of the strain gauge adhered on the quartz plate was also measured up to 10 T at 50 K, in which there was no need to calibrate the gauge resistance under the magnetic field. We have measured the gauge resistance, $R(B)$, adhered on the bulk several times, which were confirmed to be nearly the same values under identical conditions.

3. Numerical simulation framework

Based on the experimental setup shown in figure 1(a), a detailed 3D numerical model was constructed, in which OFHC Cu plates, indium sheets, bolt and nut made of stainless steel (SUS304) and Stycast™ 1266 (epoxy resin) were also added, together with the EuBaCuO bulk and the Al alloy ring. The model was equally divided into 36 elements along

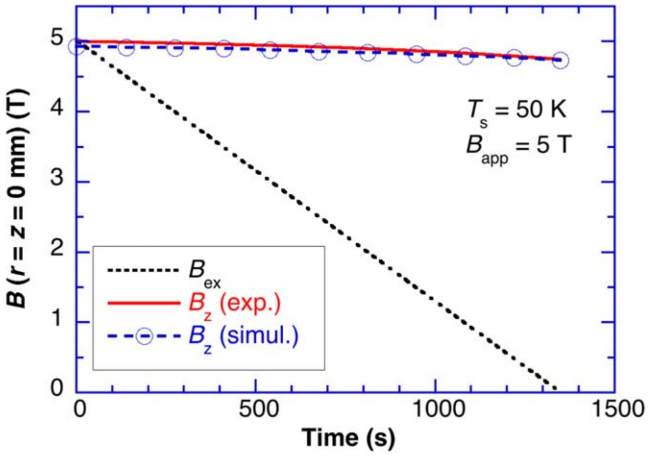

Figure 2. Experimental and simulation results of the time dependence of the trapped field, B_z, at the center of the ring bulk ($r = z = 0$) and the external field, B_{ex}, during FCM, ramped down from $B_{app} = 5$ T at 50 K.

the circumferential direction and into 1 mm intervals along the r- and z-directions, respectively. As boundary conditions, the outer surfaces of the Al-alloy ring and the Cu holder were assumed to be adiabatic and each part was fixed mechanically. The bulk was magnetized by a coil (170 mm OD, 120 mm ID, and 200 mm H), which was the same size as the superconducting solenoid coil used in the experiment.

The FCM simulation was carried out using a process identical to that described in section 2.1. The temperature of the system was set to 50 K because the maximum temperature rise during experimental FCM was as small as 1 K at the outer edge of the bulk surface. The commercial FEM software package, Photo-Eddy (Photon Ltd, Japan), was employed for the electromagnetic analysis during the FCM process. The details of fundamental equations for bulk superconductor magnetization simulations are described elsewhere [35, 36].

The nonlinear electrical properties of the superconducting bulk was described using the E–J power law

$$E = E_c\left(\frac{J}{J_c}\right)^n, \tag{3}$$

where E_c ($=10^{-4}$ V m^{-1}) is the characteristic electric field and n (=20) is a typical value for bulk REBaCuO superconductors [37, 38]. The magnetic field dependence of the critical current density, $J_c(B)$, for the bulk used in this simulation was determined using the following equation [39–41]

$$J_c(B) = J_{c1}\exp\left(-\frac{B}{B_L}\right) + J_{c2}\frac{B}{B_{max}}\exp\left[\frac{1}{k}\left(1 - \left(\frac{B}{B_{max}}\right)^k\right)\right]. \tag{4}$$

We proposed a new method to estimate the $J_c(B)$ characteristics of the bulk [29], in which the time dependence of trapped field, B_z, at the center of ring bulk during FCM was measured and fitted using the $J_c(B)$ characteristics shown in equation (4). This method can estimate the *average and macroscopic* $J_c(B)$ characteristics of the bulk without cutting and destroying the bulk.

Table 1. Numerical parameters for the $J_c(B)$ characteristics of the EuBaCuO bulk in equation (4).

	J_{c1} (A m^{-2})	B_L (T)	J_{c2} (A m^{-2})	B_{max} (T)	k
EuBaCuO bulk	1.30×10^9	0.80	1.00×10^9	4.50	1.00

Figure 2 shows the experimental and simulation results of the time dependence of B_z during FCM from 5 T at 50 K. In the experimental FCM, the external field, B_{ex}, is ramped down linearly at a rate of -0.222 T min^{-1}. B_z decreased gradually due to flux creep, and a final trapped field of 4.71 T was achieved successfully, when the B_{ex} reached zero at $t = 1350$ s. It can be seen that the simulation result of the time-dependent trapped field curve can reproduce the experimental curve by the fitting parameters shown in table 1.

The numerical simulation of the mechanical stress and strain in the bulk and Al alloy ring during FCM was carried out using the commercial FEM software, Photo-ELAS (Photon Ltd, Japan), coupled with the electromagnetic model by Photo-Eddy to incorporate Lorentz force. The bulk and Al alloy ring are assumed to be homogeneous and isotropic, and have a linear elastic response. Elastic behavior in an isotropic material can be explained by Hooke's law, in which the stress tensor, σ_{ij}, is linearly proportional to the strain tensor, ε_{ij}, as follows

$$\sigma_{ij} = \lambda \cdot \varepsilon_{kk} \cdot \delta_{ij} + 2G \cdot \varepsilon_{ij}, \tag{5}$$

$$\lambda = \frac{E \cdot \nu}{(1+\nu)(1+2\nu)}, \tag{6}$$

$$G = \frac{E}{2(1+\nu)}, \tag{7}$$

where λ and G represent the Lame's constants, δ_{ij} is the Kronecker delta function, E is the Young's modulus, and ν is the Poisson ratio of the material. In the two-dimensional model, where the mechanical stress, σ_z, along the z-direction is ignored, the mechanical strains along the θ- and r-directions are expressed in the following

$$\varepsilon_\theta = \frac{dr}{r} = \frac{(\sigma_\theta - \nu\sigma_r)}{E}, \tag{8}$$

$$\varepsilon_r = \frac{d(dr)}{dr} = \frac{(\sigma_r - \nu\sigma_\theta)}{E}, \tag{9}$$

where σ_θ and σ_r are the mechanical stress along the θ- and r-direction, respectively, and dr is the displacement along the r-direction.

The mechanical parameters, E and ν of the REBaCuO bulk, Al alloy ring (A7075-T6), epoxy resin, indium, copper (OFHC Cu) and stainless steel (SUS304) in the stress–strain analysis are summarized in table 2. The mechanical parameters of the REBaCuO bulk were assumed to be isotropic and homogeneous for simplicity.

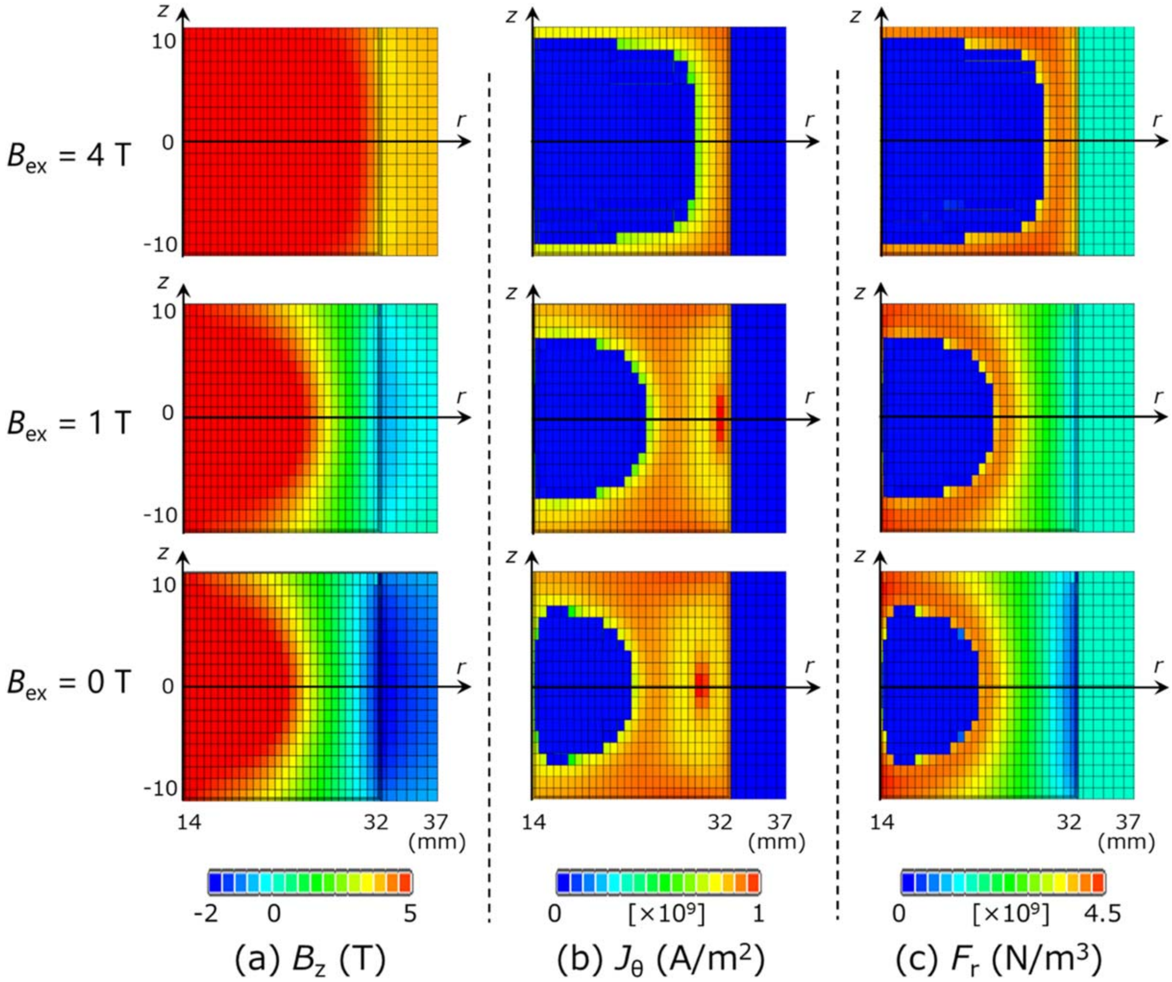

Figure 3. Simulation results of the cross-section of the ring bulk and Al alloy ring at $B_{ex} = 4$, 1 and 0 T during FCM from $B_{app} = 5$ T. The external magnetic field dependent distributions of (a) the trapped field in the *z*-direction, B_z, (left), (b) the induced current density in the θ-direction, J_θ, (middle) and (c) the Lorentz force density in the *r*-direction, F_r, (right), are shown.

4. Results and discussion

4.1. Numerical simulation results of electromagnetic properties

Figures 3(a)–(c), respectively, show simulation results of the cross-sectional profiles of the magnetic field, B_z, induced persistent current density, J_θ, and Lorentz force density, F_r, in the bulk and Al alloy ring at $B_{ex} = 4$, 1 and 0 T during FCM from $B_{app} = 5$ T. At $B_{ex} = 4$ T, the magnitude of B_z in the whole region of the ring bulk is nearly 5 T except for its outer periphery, where J_θ flows along the θ-direction only in outer region and top and bottom surfaces of the bulk. As a result, F_r is applied along the *r*-direction by the current-field interaction (i.e. $J_\theta \times B_z$). In the Al alloy ring, F_r equals to zero because $J_\theta = 0$. As the external field is ramped down, e.g. $B_{ex} = 1$ and 0 T, the region through which the persistent supercurrent flows became wider, compared to that at $B_{ex} = 4$ T. As a result, B_z in the outer region of the bulk decreased, the region with higher B_z became narrower and the B_z value at the center slightly decreased. It is obvious that the peak position of F_r shifts from the periphery to the center of the bulk with decreasing B_{ex}. When B_{ex} reaches 0 T, $B_z = 5$ T is still present in the inner central region of the bulk ($r = 17$ mm, $z = 0$ mm), and $B_z = 4.8$ T can be achieved at the center of the ring bulk ($r = z = 0$ mm), as shown in figure 2. These results suggest that the ring bulk was not fully magnetized during FCM from $B_{app} = 5$ T at 50 K due to the larger $J_c(B)$ value.

4.2. Measurement and simulation of electromagnetic strain

Figure 4(a) shows the experimental results of the external field dependence of the electromagnetic strain along the θ-direction, ε_θ, during FCM from 5 T at 50 K at each position, in which the magnetic field decreased from 5 to 0 T. The initial strain of each gauge was assumed to be zero, after the bulk was cooled from 300 to 50 K under the magnetic field of 5 T. The ε_θ value at each position monotonically increases during the ramp down of the external field, takes a maximum around $B_{ex} = 1$ T, and then slightly decreases. This trend was qualitatively similar to our previous study [32]. The ε_θ value at $r = 17$ mm is the largest, which is +0.027%, meaning the highest tensile strain in the innermost position. The ε_θ value decreases with increasing *r* in the bulk, e.g. $\varepsilon_\theta = +0.013\%$ at $r = 30$ mm. The ε_θ on the Al alloy ring ($r = 35$ mm) also see positive values during FCM, nevertheless the Lorentz force is

Table 2. Mechanical parameters (Young's modulus, E, and Poisson ratio, ν) of the EuBaCuO bulk, Al alloy (A7075-T6), epoxy resin, indium, copper (OFHC Cu) and stainless steel (SUS304) used in the simulation.

	EuBaCuO bulk	Al alloy (A7075-T6)	Epoxy	Indium	Copper (OFHC Cu)	Stainless steel (SUS304)
E (GPa)	100	78.0	3.00	12.7	125	193
ν	0.33	0.34	0.37	0.45	0.34	0.28

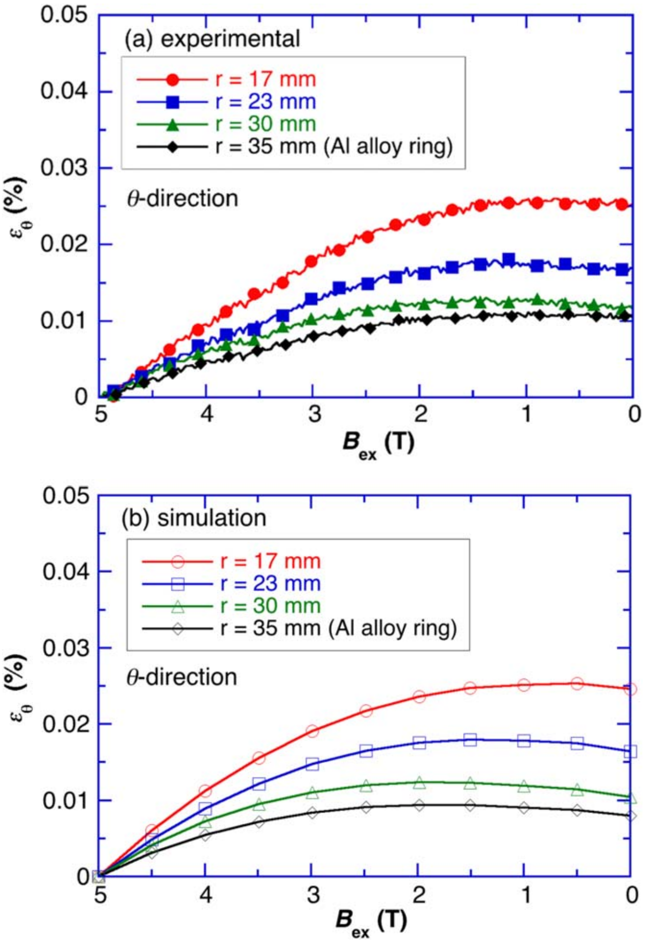

Figure 4. (a) Experimental and (b) simulation results of the electromagnetic strain along the θ-direction, ε_θ, as a function of the external field, B_{ex}, at each position on the top surface of the bulk ($r = 17$, 23 and 30 mm) and Al alloy ring ($r = 35$ mm) during FCM from $B_{app} = 5$ T at 50 K.

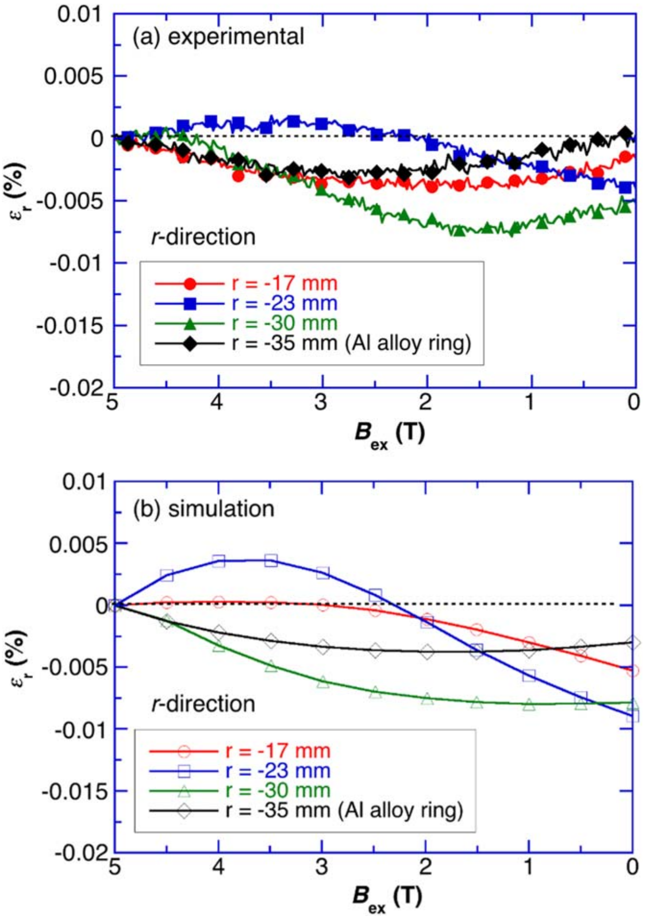

Figure 5. (a) Experimental and (b) simulation results of the electromagnetic strain along the r-direction, ε_r, as a function of the external field, B_{ex}, at each position on the top surface of the ring bulk ($r = -17$, -23 and -30 mm) and Al alloy ring ($r = -35$ mm) during FCM from 5 T at 50 K.

not produced in this region ($32 < r < 37$ mm) as shown in figure 3(c). This behavior implies that the Al alloy ring was pushed outwards from the inner bulk due to the Lorentz force and, as a result, expanded in the θ-direction.

Figure 4(b) shows the results of numerical simulation of the external field dependence of the electromagnetic strain along the θ-direction, ε_θ, during FCM from 5 T at 50 K. The simulated ε_θ data well reproduced the experimental data shown in figure 4(a) qualitatively and quantitatively. This agreement results from the reduction of the simulated ε_θ values and strongly suggests that such a realistic numerical model is necessary for the simulation to reproduce the experimental data accurately. Because the mechanical stress and strain are related three-dimensionally to each other and the electromagnetic strain is reasonably influenced by the size, shape and assumed mechanical properties of the surrounding parts.

Figure 5(a) shows the experimental results of the external field dependence of the electromagnetic strain along the r-direction, ε_r, at each measurement position, for which the magnetic field decreased from 5 to 0 T. The ε_r values at $r = -17$, -30 and -35 mm increased negatively, took a minimum, and then showed a slightly positive increase with decreasing B_{ex}, which are in clear contrast to the ε_θ values at the corresponding positions. It can be considered that the inner periphery of the ring bulk ($r = 14$ mm) and the outer periphery of the Al alloy ($r = 37$ mm) are in a 'stress-free' state, and are not restricted mechanically since there are no external stresses in the r-direction from the inner surface of the bulk and outer surface of the Al ring. Thus, the negative ε_r can be simply explained by Poisson ratio $\nu = -\varepsilon_\theta/\varepsilon_r$, and the outer boundary of superconductor bulk is pressed by the Al alloy ring. As a result, the ε_r value at $r = -30$ mm shrinks largely because the displacement at outer periphery of the ring bulk ($r = 32$ mm) is restricted due to the external compressive stress from the Al alloy ring. On the other hand, the ε_r value at $r = -23$ mm, which is an intermediate position on the ring bulk surface, shows a slight positive expansion, takes a peak, and then decreases slightly with decreasing B_{ex}. It should be noted that the maximum variation of ε_r at each position is several times smaller than ε_θ.

Figure 5(b) shows the numerical simulation results of the external field dependence of the electromagnetic strain along the r-direction, ε_r, during FCM from 5 T at 50 K. The simulated ε_r versus B_{ex} curves at $r = -23$, -30 and -35 mm reproduce the experimental data well qualitatively and quantitatively. On the other hand, the simulated ε_r versus B_{ex} curve at $r = -17$ mm exhibits a convex profile, but the experimental ε_r versus B_{ex} curve at $r = -17$ mm shown in figure 5(a) exhibits a concave one. This discrepancy may come from a difference in the load condition for the stress–strain analysis; in the actual experimental setup shown in figure 1(a), a stronger fastening torque was applied to the inner periphery of the bulk though the Cu plates along the z-direction produced from a central bolt and nut, rather than to the outer periphery, which suggest that inhomogeneous mechanical fastening pressure might be applied to the ring bulk. On the other hand, in the numerical simulation, the torque was not considered and the mechanical and thermal contact was assumed to be homogeneous. These discrepancies influence on the strain profiles, especially at the inner periphery region. However, these results of simulations and experiments are in good agreement, which suggests that the construction of a realistic FEM model and the use of realistic *average* and *macroscopic* $J_{\mathrm{c}}(B)$ characteristics for the bulk are necessary to reproduce the external field dependence of the electromagnetic strains along both directions qualitatively and quantitatively. This allows us to better understand the complex physical phenomena during magnetization process and make accurate predictions.

4.3. Estimation of electromagnetic stress using measured strains along both directions

In this subsection, we estimate the electromagnetic stresses applied to the ring bulk and Al alloy ring during FCM using the experimentally obtained strains. To estimate the stresses along both the θ- and r-directions in the bulk and Al alloy ring from the experimental strain results, the following stress–strain relationships are adopted

$$\sigma_\theta = \frac{E}{1-\nu^2}(\varepsilon_\theta + \nu\cdot\varepsilon_r), \quad (10)$$

$$\sigma_r = \frac{E}{1-\nu^2}(\varepsilon_r + \nu\cdot\varepsilon_\theta), \quad (11)$$

where $E_{\mathrm{bulk}} = 100$ GPa and $\nu_{\mathrm{bulk}} = 0.33$ are assumed in the ring bulk region, and $E_{\mathrm{Al}} = 78.0$ GPa and $\nu_{\mathrm{Al}} = 0.34$ are assumed in the Al alloy region, as shown in table 2. These equations are obtained from Hooke's law for an isotropic material within its elastic range, in which the stress along the z-direction, σ_z, in the materials is assumed to be zero. This assumption was used previously in the analytical calculations for the stress–strain relationship for a ring-shaped bulk superconductor [22].

Figure 6(a) shows the estimated results of the electromagnetic stress along the θ-direction, σ_θ, as a function of the external field, B_{ex}, at each measurement position during FCM from 5 T at 50 K, which were obtained using equation (10) and the experimental strain values shown in figures 4(a) and 5(a). Estimated σ_θ values at each position increase, take a maximum at an intermediate B_{ex}, and then slightly decrease as the external field is ramped down. The σ_θ value at $r = 17$ mm is higher, compared to those at the other positions and at any B_{ex}. Its maximum is estimated to be +29 MPa at $B_{\mathrm{ex}} = 1$ T, meaning that the tensile stress concentration occurs at the inner periphery, which are similar to the results for ε_θ shown in figure 4(a). These trends have been reported in our previous works [25–29, 42].

Figure 6(b) shows the simulation results of the electromagnetic stress along the θ-direction, σ_θ, as a function of the external field, B_{ex}, at each measurement position during FCM from 5 T at 50 K, for which the numerical simulation was performed only using the electromagnetic and mechanical analyses. The numerical simulation results are in good agreement with the estimation using the measured results qualitatively and quantitatively. A maximum stress of +28 MPa was observed at $r = 17$ mm, which is in excellent agreement with estimated results for the maximum stress at same position. The fracture strength of a typical Ag-doped REBaCuO bulk is considered to be 50–70 MPa [43–45]. In this sense, the present FCM conditions can avoid the mechanical fracture. Figure 6(c) shows the σ_θ distribution in the ring bulk ($14 < r < 32$ mm) and Al alloy ring ($32 < r < 37$ mm) at $B_{\mathrm{ex}} = 1$ T. The σ_θ distribution in the ring bulk is inhomogeneous and σ_θ is concentrated at the innermost edge of the ring bulk surface. These results suggest that the electromagnetic stress takes a maximum at the innermost edge of the ring bulk surface, and that the electromagnetic strain also takes a maximum at the same position.

Figures 7(a) and (b), respectively, show the estimated and simulated results of the electromagnetic stresses along the r-direction, σ_r, as a function of the external field, B_{ex}, at each measurement position during FCM from 5 T at 50 K, for which the estimated results were obtained using equation (11) and the experimental strain values shown in figures 4(a) and 5(a). The estimated σ_r values at $r = -23$, -30, and -35 mm were reproduced well by the numerical simulation. The estimated σ_r versus B_{ex} curve at $r = -17$ mm was not necessarily consistent with the simulation curve, which may result from the similar cause as that for the strain measurement as shown in figure 5(a). Figure 7(c) shows the σ_r distribution in the ring bulk ($14 < r < 32$ mm) and the Al alloy ring ($32 < r < 37$ mm) at $B_{\mathrm{ex}} = 1$ T. The σ_r distribution in the ring bulk is inhomogeneous and σ_r is concentrated at the

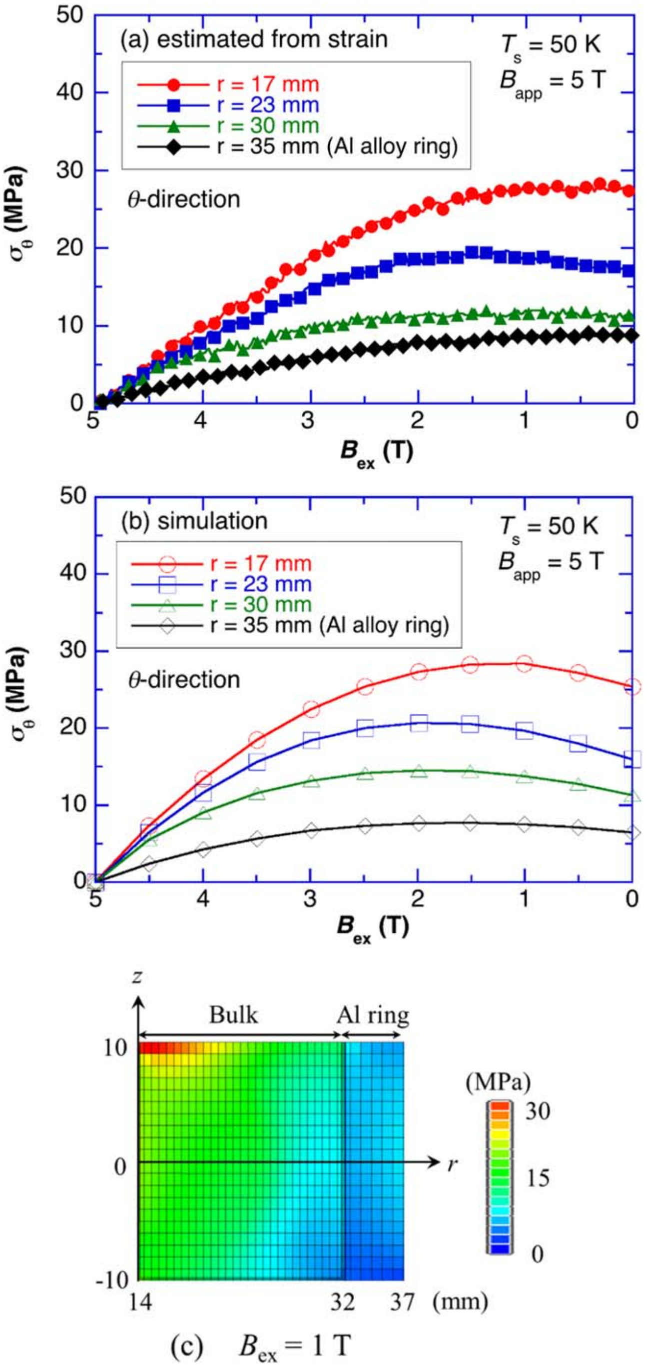

Figure 6. (a) Estimated and (b) numerical simulation results for the mechanical stress, σ_θ, along the θ-direction, as a function of the external field, B_{ex}, at each of the measurement positions during FCM from 5 T at 50 K. (c) The σ_θ distribution in the bulk and Al alloy ring at $B_{ex} = 1$ T.

innermost edge of the ring bulk surface. The maximum σ_r value is smaller than 10 MPa, which is much smaller than the fracture strength. Thus, the ring bulk did not fracture during FCM from 5 T.

5. Conclusion

Two-directional strain measurement has been shown to be a valuable method to estimate precise mechanical stresses,

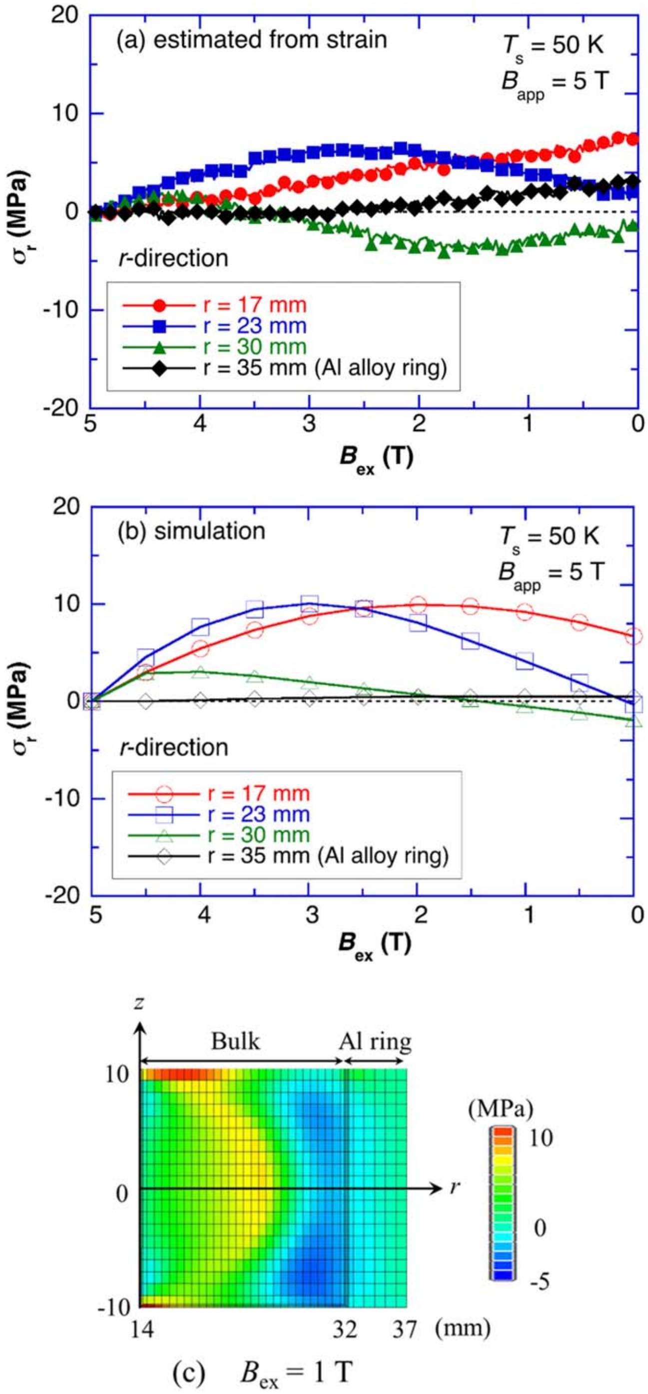

Figure 7. (a) Estimated and (b) numerical simulation results of the mechanical stress, σ_r, along the r-direction, as a function of the external field, B_{ex}, at each measurement position during FCM from 5 T at 50 K. (c) The σ_r distribution in the bulk and Al alloy ring at $B_{ex} = 1$ T.

which cannot be directly measured. We have simultaneously measured electromagnetic strains along both the θ- and r-directions on a large single-grain EuBaCuO ring bulk, reinforced by an Al alloy ring, during FCM from $B_{app} = 5$ T at 50 K using several strain gauges. A 3D finite element model that represents the exact experimental setup was constructed, including not only the ring bulk and Al alloy ring, but also the sample holder and mechanical support structure (OFHC Cu plates, indium sheets, bolt and nut made of stainless steel (SUS304) and Stycast™ 1266 (epoxy resin)), with excellent qualitative and quantitative agreement. The important results and conclusions of this study are summarized as follows.

(1) The electromagnetic strain along the θ-direction, ε_θ, takes a maximum at an intermediate external field and is the largest at the innermost position of the bulk surface, decreasing with increasing radius. The electromagnetic strain along the r-direction, ε_r, is several times smaller than the ε_θ, and has a contrasting B_{ex} dependence at each position along the bulk surface.

(2) The simulation results of the electromagnetic strains along both directions show excellent qualitative and quantitative agreement with the experimental ones. In the numerical simulation, the construction of a realistic model based on all parts of the actual experimental setup is necessary to reproduce the experimental results precisely. The quantitative agreement between the experiments and simulations validate both our experimental and simulation techniques, and this numerical simulation framework can be used as a reliable tool to investigate the possibility of mechanical fracture of bulk superconductors for any bulk superconducting material and geometry or magnetizing process.

(3) The electromagnetic stresses, σ_θ and σ_r, along both directions are estimated during the FCM process from the experimentally obtained strains, ε_θ and ε_r, using Hooke's law. The consistency of the experimental and numerical results suggests that this kind of strain measurement can estimate electromagnetic stresses precisely and is an effective technique for the evaluation of the mechanical properties of bulk superconductors during FCM to clarify the possibility of mechanical fracture.

Acknowledgments

This research is partially supported by a 'Development of Systems and Technologies for Advanced Measurement and Analysis' from Japan Agency for Medical Research and Development, AMED and by JSPS KAKENHI Grant Nos. 15K04646 and 19K05240. M D Ainslie would like to acknowledge financial support from an Engineering and Physical Sciences Research Council (EPSRC) Early Career Fellowship, EP/P020313/1. All data are provided in full in the results section of this paper.

ORCID iDs

Sora Namba https://orcid.org/0000-0001-7268-5326
Hiroyuki Fujishiro https://orcid.org/0000-0003-1483-835X
Tomoyuki Naito https://orcid.org/0000-0001-7594-3466
Mark D Ainslie https://orcid.org/0000-0003-0466-3680
Kai Y Huang https://orcid.org/0000-0001-7476-305X

References

[1] Gotoh S, Murakami M, Fujimoto H and Koshizuka N 1992 *J. Appl. Phys.* **72** 2404–10
[2] Zhou D, Izumi M, Miki M, Felder B, Ida T and Kitano M 2012 *Supercond. Sci. Technol.* **25** 103001
[3] Hayashi H, Tsutsumi K, Saho N, Nishijima N and Asano K 2003 *Physica* C **392–396** 745–8
[4] Werfel F N, Floegel-Delor U, Rothfeld R, Riedel T, Goebel B, Wippich D and Schirrmeister P 2012 *Supercond. Sci. Technol.* **25** 014007
[5] Fuchs G *et al* 2013 *Supercond. Sci. Technol.* **26** 122002
[6] Weiss J D, Yamamoto A, Polyanskii A A, Richardson R B, Larbalestier D C and Hellstrom E E 2015 *Supercond. Sci. Technol.* **28** 112001
[7] Bean C P 1962 *Phys. Rev. Lett.* **8** 250
[8] Ren Y, Weinstein R, Liu J, Sawh R P and Foster C 1995 *Physica* C **251** 15–26
[9] Fuchs G, Schätzle P, Krabbes G, Gruß S, Verges P, Müller K-H, Fink J and Schultz L 2000 *Appl. Phys. Lett.* **76** 2107–9
[10] Nariki S, Sakai N and Murakami M 2005 *Supercond. Sci. Technol.* **18** S126–30
[11] Durrell J H *et al* 2014 *Supercond. Sci. Technol.* **27** 082001
[12] Tomita M and Murakami M 2003 *Nature* **421** 517–20
[13] Nakamura T, Tamada D, Yanagi Y, Itoh Y, Nemoto T, Utumi H and Kose K 2015 *J. Magn. Reson.* **259** 68–75
[14] Ogawa K, Nakamura T, Terada Y, Kose K and Haishi T 2011 *Appl. Phys. Lett.* **98** 234101
[15] Nariki S, Sakai N, Tomita M and Murakami M 2002 *Physica* C **378–381** 779–82
[16] Fujimoto H, Murakami A, Teshima H and Morita M 2013 *Cryogenics* **57** 6–11
[17] Konstantopoulou K, Shi Y H, Dennis A R, Durrell J H, Pastor J Y and Cardwell D A 2014 *Supercond. Sci. Technol.* **27** 115011
[18] Huang K Y *et al* 2018 *IEEE Trans. Appl. Supercond* **28** 6801505
[19] Sakai N, Mase A, Ikuta H, Seo S J, Mizutani U and Murakami M 2000 *Supercond. Sci. Technol.* **13** 770–3
[20] Murakami A *et al* 2003 *Cryogenics* **43** 345–50
[21] Johansen T, Wang C, Chen Q Y and Chu W–K 2000 *J. Appl. Phys.* **88** 2730–3
[22] Johansen T 2000 *Supercond. Sci. Technol.* **13** R121–37
[23] Huang C, Yong H and Zhou H 2013 *Supercond. Sci. Technol.* **26** 105007
[24] Johansen T H, Chen Q Y and Chu W-K 2001 *Physica* C **349** 201–10
[25] Fujishiro H, Ainslie M D, Takahashi K, Naito T, Yanagi Y, Itoh Y and Nakamura T 2017 *Supercond. Sci. Technol.* **30** 085008
[26] Takahashi K, Fujishiro H, Naito T, Yanagi Y, Itoh Y and Nakamura T 2017 *Supercond. Sci. Technol.* **30** 115006
[27] Takahashi K, Fujishiro H, Naito T, Yanagi Y, Itoh Y and Nakamura T 2018 *IEEE Trans. Appl. Supercond.* **28** 6800705
[28] Fujishiro H, Takahashi K, Naito T, Yanagi Y, Itoh Y and Nakamura T 2018 *Physica* C **550** 52
[29] Fujishiro H, Naito T, Yanagi Y, Itoh Y and Nakamura T 2019 *Supercond. Sci. Technol.* **32** 065001
[30] Fujishiro H, Naito T and Awaji S 2019 *Supercond. Sci. Technol.* **32** 045005
[31] Miyamoto T, Nagashima K, Sakai N and Murakami M 2000 *Physica* C **340** 41–50
[32] Takahashi K, Namba S, Fujishiro H, Naito T, Yanagi Y, Itoh Y and Nakamura T 2019 *Supercond. Sci. Technol.* **32** 015007
[33] Morita M, Sawamura M, Takebayashi S, Kimura K, Teshima H, Tanaka M, Miyamoto K and Hashimoto M 1994 *Physica* C **235–240** 209–12

[34] Nariki S, Teshima H and Morita M 2016 *Supercond. Sci. Technol.* **29** 034002
[35] Fujishiro H, Itoh Y, Yanagi Y and Nakamura T 2015 *Supercond. Sci. Technol.* **28** 095018
[36] Ainslie M D and Fujishiro H 2015 *Supercond. Sci. Technol.* **28** 053002
[37] Ainslie M D, Srpcic J, Zhou D, Fujishiro H, Takahashi K, Cardwell D A and Durrell J H 2018 *IEEE Trans. Appl. Supercond.* **28** 6800207
[38] Zhou D *et al* 2018 *Supercond. Sci. Technol.* **31** 105005
[39] Jirsa M, Půst L, Dlouhý D and Koblischka M R 1997 *Phys. Rev.* B **55** 3276–84
[40] Muralidhar M, Sakai N, Jirsa M, Koshizuka N and Murakami M 2004 *Appl. Phys. Lett.* **85** 3504
[41] Kii T *et al* 2012 *IEEE Trans. Appl. Supercond.* **22** 4100904
[42] Ainslie M D, Huang K Y, Fujishiro H, Chaddock J, Takahashi K, Namba S, Cardwell D A and Durrell J H 2019 *Supercond. Sci. Technol.* **32** 034002
[43] Lee D and Salama K 1990 *Japan. J. Appl. Phys.* **29** L2017–9
[44] Matsui M, Sakai N and Murakami M 2002 *Supercond. Sci. Technol.* **15** 1092–8
[45] Katagiri K, Murakami A, Kan R, Kasaba K, Noto K, Muralidhar M, Sakai N and Murakami M 2003 *Physica* C **392-396** 526–30